PHYSICAL REVIEW C, VOLUME 65, 064603

Projectile fragmentation of ^{112}Sn at $E_{\mathrm{lab}}=1A$ GeV

A. Stolz,* T. Faestermann, J. Friese, P. Kienle, H.-J. Körner, M. Münch, R. Schneider, E. Wefers, and K. Zeitelhack
Physikdepartment E12, Technische Universität München, D-85748 Garching, Germany

K. Sümmerer, H. Geissel, J. Gerl, G. Münzenberg, C. Schlegel, R. S. Simon, and H. Weick
Gesellschaft für Schwerionenforschung, D-64291 Darmstadt, Germany

M. Hellström and M. N. Mineva
Division of Cosmic and Subatomic Physics, Physics Department, Lund University, S-221 00 Lund, Sweden

P. Thirolf
Sektion Physik der Ludwig-Maximilians-Universität München, D-85748 Garching, Germany

(Received 10 February 2002; published 22 May 2002)

We have measured production cross sections of projectilelike fragments in the reaction of neutron-deficient ^{112}Sn with a ^{9}Be target at an energy of $E_{\mathrm{lab}}=1A$ GeV. Results have been obtained for neutron-deficient products along the $N=Z$ line down to the subnanobarn range. We find very good agreement with the recently revised empirical parametrization EPAX. In addition, a few one- and two-proton pickup cross sections have been measured. The former ones are well reproduced by intranuclear-cascade calculations.

DOI: 10.1103/PhysRevC.65.064603 PACS number(s): 25.70.Mn, 25.75.−q

I. INTRODUCTION

One of the regions of the nuclear chart that is currently explored extensively in both experimental and theoretical studies is the region along the $N=Z$ line near and below ^{100}Sn. On the one hand, this is based on the interest in studying directly the doubly magic nucleus ^{100}Sn, a key nucleus for the investigation of Gamov-Teller β decay [1]. On the other hand, the nuclei below ^{100}Sn along the $N=Z$ line are also of interest for studies of the superallowed Fermi β decay [2] and for the astrophysical rp process [3].

To produce the nuclei to be studied in this region, low-energy fusion-evaporation reactions have been applied successfully for many years. Recently, also high- and intermediate-energy fragmentation reactions have proved to be a valuable production mechanism. They were successful, e.g., in identifying ^{100}Sn for the first time [4–6] or in studying half-lives and decay branchings of neutron-deficient nuclei along the $N=Z$ line [7,8].

The SIS/FRS facility at GSI allows us to use projectile fragmentation at incident energies around $1A$ GeV to produce the nuclei of interest. One key requisite for the planning of such experiments is knowledge of the respective production cross sections. In particular, one needs to know the production cross sections for the most neutron-deficient beams because with their use one expects enhanced yields of the most neutron-deficient fragment nuclei, compared to those from beams near the valley of β stability. At SIS energies, data are at present only available for ^{124}Xe and ^{58}Ni projectiles [9,5].

The present study has been performed to extend the current database by studying the fragmentation of the most neutron-deficient tin isotope ^{112}Sn. This isotope was used for studies at GANIL to produce ^{100}Sn at the intermediate energy of $63A$ MeV, and a production cross section for ^{100}Sn of $\sigma \geqslant 120$ pb was given in Ref. [10]. This cross section is much larger than the one found in the earlier high-energy GSI experiment using a $1A$ GeV ^{124}Xe beam, where a cross section for ^{100}Sn of 11 ± 4 pb was measured [4]. To profit from this expected enhancement, we started another investigation of ^{100}Sn and neighboring nuclei at GSI using also a ^{112}Sn beam. In this paper we will present the systematics of production cross sections of neutron-deficient Sn to Sr isotopes. The results will be discussed in the framework of empirical cross-section parametrizations. Results from spectroscopic studies of these nuclei will be presented in forthcoming papers.

II. EXPERIMENTAL PROCEDURE

The experiment was performed at the fragment separator facility FRS of GSI at Darmstadt, Germany. A beam of ^{112}Sn was accelerated to an energy of $1015A$ MeV in the heavy-ion synchrotron SIS after 20 injection and cooling cycles. Spills with intensities of up to 5×10^{8} ions lasting for 4 s with a repetition rate of 1 in 14 s were focused onto a 4007 mg/cm^2 beryllium target in front of the fragment separator FRS [11]. With a total nuclear reaction cross section of $\sigma_{\mathrm{total}}=2.2$ b calculated from an empirical parametrization [12] the total reaction probability of the primary beam in this target was 45%.

The experimental setup is sketched in Fig. 1. The primary beam intensity was determined from the current induced by delta electrons in a titanium converter foil (SEETRAM [13]) in front of the target. This detector has an areal thickness of 18 mg/cm^2. The SEETRAM beam intensity monitor was calibrated at low beam currents ($\leqslant 2\times10^{5}$ ions/s) by counting individual beam particles with a scintillator which could

---

*Present address: National Superconducting Cyclotron Laboratory, Michigan State University, East Lansing, MI 48824.

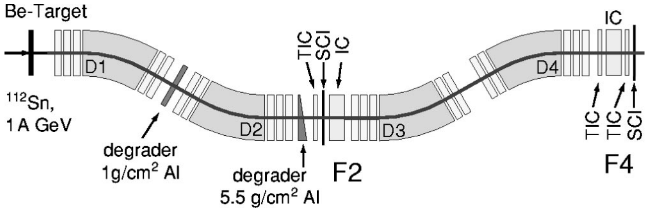

FIG. 1. Experimental setup at the FRS at GSI. The detector systems for the fragment identification were positioned at the momentum-dispersive (F2) and the achromatic (F4) focal planes: tracking ionization chamber (TIC), ionization chamber for charge identification (IC), plastic scintillator (SCI).

be moved into the beam. At high beam currents it was calibrated with the scintillator at the intermediate focal plane taking into account the total reaction rate in the degrader matter. We estimate the error of the beam intensity to be 30%, resulting from both the systematic calibration error and the counting statistics of the SEETRAM current digitizer.

The fragments were isotopically separated in the FRS by a combination of magnetic deflection and energy losses caused by a 1 g/cm^2 Al degrader inserted after the first 30° deflecting magnet (D1) and a 5.5 g/cm^2 Al degrader in the intermediate focal plane after the second 30° magnet (D2). Detector systems placed in front of the third (D3) and behind the fourth 30° magnets (D4) allowed the determination of the fragment trajectories using position-sensitive ionization chambers and the time of flight between a start and a stop plastic scintillator. The fragment nuclear charge number Z was determined by an energy-loss measurement in ionization chambers at the intermediate and the final focal plane. The two independent measurements allowed suppression of particles resulting from reactions in the second half of the separator.

The ionization chamber at the intermediate focal plane F2 had an active length of 400 mm segmented into eight anode strips. To achieve a high rate capability up to 2×10^5 ions per second, fast (electron drift velocity $v_d=11\,\mathrm{cm}/\mu s$) and dense gas CF$_4$ at atmospheric pressure and a small drift gap of 40 mm were used. The total active area of 200×40 mm^2 is adapted to the geometrical size of the F2 focal plane of the FRS. For fragments in the region $Z=35-50$ a nuclear charge resolution of $\Delta Z=0.26$ [full width at half maximum (FWHM)] was achieved (see Fig. 2). At a rate of 100 kHz a fraction of 3% of the events with an increased pulse height due to pileup was observed. These events could be discarded using a fast scintillator signal ($\Delta t=5$ ns) for pileup rejection.

The ionization chamber at the final focal plane F4 had an active length of 400 mm with fourfold segmentation and was operated with argon-methane gas (90/10) at atmospheric pressure. A nuclear charge resolution of $\Delta Z=0.35$ (FWHM) was achieved. At the fragment energy after the degrader ($\approx 750A$ MeV) 99% of the ions are fully ionized ($q=Ze$) [14]. Thus this measurement also determines the nuclear charge of the fragments. Both detectors were calibrated with the primary beam for the nuclear charge number $Z=50$ (see Fig. 2).

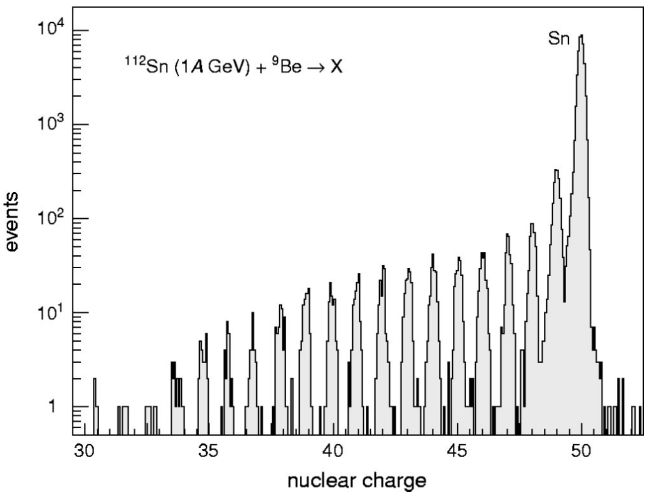

FIG. 2. Nuclear charge spectrum of fragments from ^{112}Sn fragmentation at 1*A* GeV, measured in an ionization chamber operated with CF$_4$ at atmospheric pressure. The primary beam with $Z=50$ was used for calibration.

In the momentum-dispersive intermediate focal plane (F2) the positions of the fragments and thus their magnetic rigidities were measured using a tracking ionization chamber with a highly segmented cathode and single-strip readout. This chamber had an active area of 200×60 mm^2 and a drift length of 10 mm in the direction of the beam. The chamber was operated with CF$_4$ gas at atmospheric pressure. The position resolution was determined by the strip pitch of 1.75 mm. The strips were read out by integrated GASSIPLEX chips [15], which each consists of 16 preamplifiers, shapers, a track-and-hold stage, and an analog multiplexer.

In addition, a fast but low-resolution ($\sigma_x=4.3$ mm) position determination with a plastic scintillator allowed us to reject most of the double hits occurring at the intermediate focal plane.

At the final focal plane (F4) two similar tracking ionization chambers with a strip pitch of 1 mm were used to determine both the position and the angle. These chambers, separated by a distance of 1035 mm, provided an angular resolution of 1.5 mrad, allowing the complete reconstruction of the track through the separator.

The magnetic dipole fields were measured by Hall probes with an relative accuracy of $\Delta B/B=10^{-4}$. The dispersion in the central focal plane F2 was determined to be $\Delta x/(\Delta B\rho/B\rho_0)=65.3$ mm/% by measuring the position of the primary beam for several field settings. With a beam spot size of $\Delta x\approx 2.5$ mm at the target and a position resolution of the ionization chamber at the intermediate focal plane F2 of $\Delta x=1.2$ mm (FWHM) this allowed us to determine the momentum of fragments with known ionic charge with a resolution of $\Delta p/p=3.1\times10^{-4}$.

For the measurement of the time of flight, 2-mm-thick plastic scintillators (BC-420) were mounted at the focal planes F2 and F4 of the FRS. The length of the flight path between the scintillators was 35 m. The scintillation light was detected on either side by fast photomultipliers (Hamamatsu R2083) separated 10 cm from the scintillator edges realizing a time resolution of $\Delta(t_{\mathrm{left}}-t_{\mathrm{right}})=115$ ps

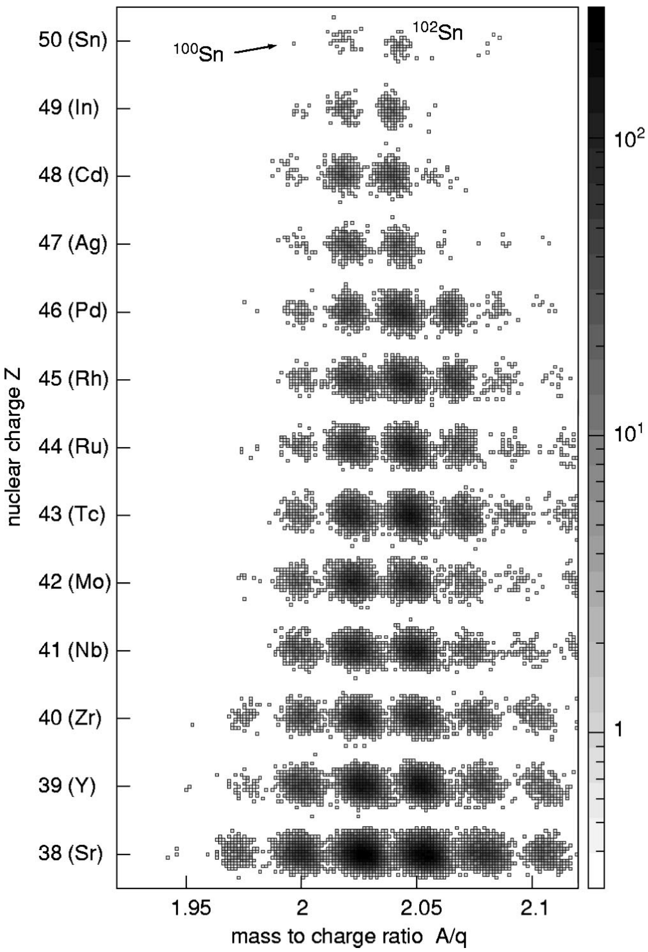

FIG. 3. Identification plot of fragments from ^{112}Sn fragmentation at 1A GeV. Results of several field settings of the fragment separator have been plotted on top of each other. A nuclear charge resolution of $\Delta Z = 0.23$ (FWHM) and a mass resolution of $\Delta A = 0.32$ (FWHM) have been achieved.

(FWHM) for the centered primary beam. The scintillator at the final focal plane provided also the trigger for the readout.

Together with the magnetic rigidity and energy-loss measurements, the fragments could be identified with respect to nuclear charge and mass number. As the spectrometer acceptance is about ±1% in momentum, several field settings were necessary to cover the neutron-deficient area of the nuclear chart along the $N=Z$ line.

III. RESULTS

A. Isotope identification

Figure 3 represents an identification plot showing the nuclear charge Z plotted versus the mass to charge ratio A/q. In this figure, the results of several field settings of the fragment separator have been plotted on top of each other. For each individual setting, mainly nine nuclides are transported to the final focal plane due to the acceptance of the spectrometer.

The arithmetic mean of the two velocity-corrected measurements of the energy loss in the ionization chambers at both focal planes resulted in a nuclear charge resolution of $\Delta Z = 0.23$ (FWHM).

By using the tracking ionization chambers to determine the track of the fragments through the separator and two independent measurements of the time of flight we achieved a mass resolution of $\Delta A = 0.32$ (FWHM).

The detection efficiencies of the detectors for position and nuclear charge measurement could be determined by comparing to the scintillator detectors. Including the dead time of the data acquisition the total identification efficiency for nuclear charges $Z > 35$ was determined to be 75%–95%.

B. Determination of cross sections

Individual isotopic cross sections were calculated from the numbers of counts fulfilling a two-dimensional 3σ window condition in spectra where the nuclear charge Z is plotted versus the mass-to-charge ratio A/q (see Fig. 3). Assuming a 10-times higher rate for a neighboring isotope the probability for misidentification is below 2%. In the case of very low statistics for identified nuclei the statistical error intervals given in [16] were used.

As a result of the mostly small numbers of total counts per fragment, the ion-optical transmission could not be determined reliably by a measurement of the momentum distribution at the intermediate focal plane. Therefore a Monte Carlo simulation [17] of the spectrometer transmission was used. For the central fragment of each tune of the FRS the ion-optical transmission was calculated to be above 90%. Including losses due to secondary reactions in the degrader matter and ionic-charge changes the total transmission was still above 50%. For the central fragment an uncertainty of 20% in the transmission was assumed for noncentral fragments up to 40%. Isotopes with a low transmission could often be observed in two adjacent field settings, thus minimizing the error resulting from the uncertainty in the transmission.

Cross sections down to 1 pb could be determined in the mass region $77 \leqslant A \leqslant 111$ with nuclear charge numbers $40 \leqslant Z \leqslant 52$. During a 62-h run with an integrated primary beam intensity of 8×10^{12} ions one ^{100}Sn nucleus could be identified. In the more typical case of ^{90}Rh a total number of 61 ions were collected within a measurement time of 4.2 h. All derived cross sections are given in Tables I and II.

IV. DISCUSSION

A. Cross sections of nucleon-removal products

The isotopic distributions for the elements Sn to Sr measured in the current experiment are shown in Figs. 4 and 5. They represent typical “fragmentation” cases, where nucleons have been abraded and/or evaporated from the ^{112}Sn projectile. Since our study was aimed at isotopes close to the $N=Z$ line, only a limited range of masses on the neutron-deficient side was selected by the FRS. Typically, the cross sections are in the μb–nb range, with the smallest cross section measured for ^{100}Sn as $\sigma_{112} = 1.8^{+3.2}_{-1.3}$ pb. This value is lower than the one measured in the reaction of 1.1A GeV ^{124}Xe with ^{9}Be, $\sigma_{124} = 11 \pm 4$ pb, and far below the value of

TABLE I. Measured production cross sections for the respective fragments formed in the reaction of ^{112}Sn(1015A MeV)+^{9}Be.

El.	Z	A	σ [b]	El.	Z	A	σ [b]
Sn	50	100	$(1.8^{+3.2}_{-1.3})\times10^{-12}$	Pd	46	92	$(1.0^{+0.6}_{-0.5})\times10^{-09}$
Sn	50	101	$(2.1\pm0.9)\times10^{-10}$	Pd	46	93	$(2.4\pm1.0)\times10^{-08}$
Sn	50	102	$(7.0\pm2.6)\times10^{-09}$	Pd	46	94	$(4.1\pm1.7)\times10^{-07}$
Sn	50	103	$(1.7\pm0.8)\times10^{-07}$	Rh	45	90	$(1.6\pm0.7)\times10^{-09}$
Sn	50	104	$(2.1\pm0.9)\times10^{-06}$	Rh	45	91	$(3.6\pm1.5)\times10^{-08}$
Sn	50	105	$(2.5\pm1.1)\times10^{-05}$	Rh	45	92	$(7.0\pm2.9)\times10^{-07}$
Sn	50	106	$(1.4\pm0.8)\times10^{-04}$	Ru	44	87	$(2.5^{+2.2}_{-1.9})\times10^{-10}$
Sn	50	107	$(8.7\pm5.2)\times10^{-04}$	Ru	44	88	$(2.8\pm1.2)\times10^{-09}$
Sn	50	108	$(4.1\pm1.7)\times10^{-03}$	Ru	44	89	$(7.5\pm3.1)\times10^{-08}$
Sn	50	109	$(1.0\pm0.5)\times10^{-02}$	Ru	44	90	$(1.2\pm0.5)\times10^{-06}$
In	49	98	$(4.8^{+2.8}_{-2.5})\times10^{-11}$	Tc	43	86	$(5.3\pm2.3)\times10^{-09}$
In	49	99	$(1.2\pm0.5)\times10^{-09}$	Tc	43	87	$(1.1\pm0.5)\times10^{-07}$
In	49	100	$(2.8\pm1.2)\times10^{-08}$	Mo	42	83	$(3.5^{+2.2}_{-2.0})\times10^{-10}$
In	49	101	$(6.7\pm3.0)\times10^{-07}$	Mo	42	84	$(1.1\pm0.5)\times10^{-08}$
In	49	102	$(5.3\pm2.2)\times10^{-06}$	Mo	42	85	$(2.4\pm1.0)\times10^{-07}$
In	49	103	$(5.6\pm2.5)\times10^{-05}$	Nb	41	82	$(1.6\pm0.7)\times10^{-08}$
In	49	104	$(3.1\pm1.9)\times10^{-04}$	Nb	41	83	$(3.0\pm1.3)\times10^{-07}$
In	49	105	$(1.9\pm1.1)\times10^{-03}$	Zr	40	78	$(2.7^{+4.9}_{-2.0})\times10^{-11}$
In	49	106	$(4.4\pm1.9)\times10^{-03}$	Zr	40	79	$(1.2^{+0.7}_{-0.6})\times10^{-09}$
In	49	107	$(1.1\pm0.5)\times10^{-02}$	Zr	40	80	$(2.5\pm1.1)\times10^{-08}$
Cd	48	96	$(3.0\pm1.4)\times10^{-10}$	Zr	40	81	$(7.0\pm2.9)\times10^{-07}$
Cd	48	97	$(5.7\pm2.4)\times10^{-09}$	Y	39	76	$(2.6^{+4.7}_{-2.0})\times10^{-11}$
Cd	48	98	$(1.0\pm0.4)\times10^{-07}$	Y	39	77	$(6.5\pm2.7)\times10^{-10}$
Cd	48	99	$(2.1\pm0.9)\times10^{-06}$	Y	39	78	$(3.5\pm1.5)\times10^{-08}$
Ag	47	96	$(1.9\pm0.8)\times10^{-07}$	Y	39	79	$(7.3\pm3.1)\times10^{-07}$
Ag	47	97	$(3.7\pm1.7)\times10^{-06}$	Sr	38	74	$(4.9^{+4.0}_{-2.9})\times10^{-10}$
Ag	47	94	$(3.7^{+2.0}_{-1.9})\times10^{-10}$	Sr	38	75	$(6.5\pm2.9)\times10^{-09}$
Ag	47	95	$(9.0\pm3.9)\times10^{-09}$	Sr	38	76	$(8.2\pm3.4)\times10^{-08}$
Pd	46	91	$(9.5^{+17}_{-7.1})\times10^{-11}$	Sr	38	77	$(1.9\pm0.8)\times10^{-06}$

$\geqslant$120 pb from the GANIL measurement mentioned above. We will discuss this in more detail below.

In Figs. 4 and 5 our data are compared to predictions from an empirical parametrization of high-energy fragmentation cross sections, EPAX [18] (solid lines in the figures). In general, the distributions are well reproduced, in particular when considering the range of orders of magnitudes spanned by the data. One should note, however, that preliminary results for Sn isotopes from the present study were used to find an improved parametrization of the "memory effect" for neutron-deficient projectiles in the EPAX formula; thus, the comparison for Sn cannot be regarded as an unbiased check of the validity of the EPAX formula. The other cross sections (In to Sr isotopes) were not used in fitting the parameters.

TABLE II. Measured production cross sections for ($Z_{\mathrm{proj}}+1$) and ($Z_{\mathrm{proj}}+2$) fragments formed in the reaction ^{112}Sn(1015A MeV)+^{9}Be and ^{112}Sn(1015A MeV)+$^{\mathrm{nat}}$Cu.

			^{112}Sn+ ^{9}Be	^{112}Sn+ $^{\mathrm{nat}}$Cu
El.	Z	A	σ [b]	σ [b]
Sb	51	106	$(1.6\pm0.7)\times10^{-07}$	$(2.0\pm0.9)\times10^{-07}$
Sb	51	107	$(2.8\pm1.2)\times10^{-06}$	$(4.2\pm1.8)\times10^{-06}$
Sb	51	108	$(1.2\pm0.5)\times10^{-05}$	–
Sb	51	109	$(1.3\pm0.6)\times10^{-04}$	–
Te	52	108	$(3.1^{+1.7}_{-1.4})\times10^{-09}$	$(1.2^{+2.1}_{-0.9})\times10^{-09}$
Te	52	109	$(1.4\pm0.6)\times10^{-08}$	$(3.9\pm1.8)\times10^{-08}$
Te	52	110	$(7.2\pm2.9)\times10^{-08}$	–
Te	52	111	$(1.5\pm0.7)\times10^{-07}$	–

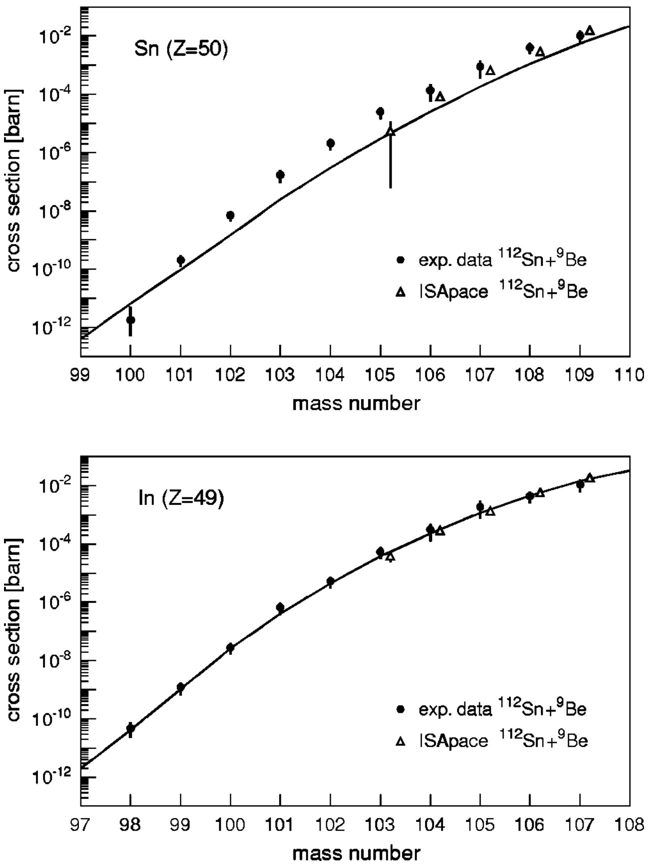

FIG. 4. Production cross sections of tin and indium istopes for nucleon-removal channels from the reaction 1A GeV ^{112}Sn+^{9}Be. The solid lines indicate the prediction from the EPAX parametrization [18]. Open symbols represent calculated cross sections from the ISApace INC plus evaporation model [19].

While an analytical function like EPAX is useful to predict production cross sections in high-energy heavy-ion reactions, it is not related to any physical model and thus does not yield insight into the underlying physics of such reactions. For a more physical understanding of the processes, we have applied a combination of an intranuclear-cascade model ISABEL [20] and a thermal-evaporation model PACE [21] to the present reaction. This package, termed "ISApace" in the following, has been applied successfully, e.g., to the reactions of ^{136}Xe+^{9}Be and ^{197}Au+^{27}Al, both at energies around 1A GeV [22]. Cross sections and momentum distributions of proton-removal products could be well reproduced. In addition, we could show that for the reaction of 0.8A GeV ^{129}Xe+^{27}Al the formation of nuclear-charge pickup products (isotopes of $_{55}$Cs) was correctly calculated by ISApace [19].

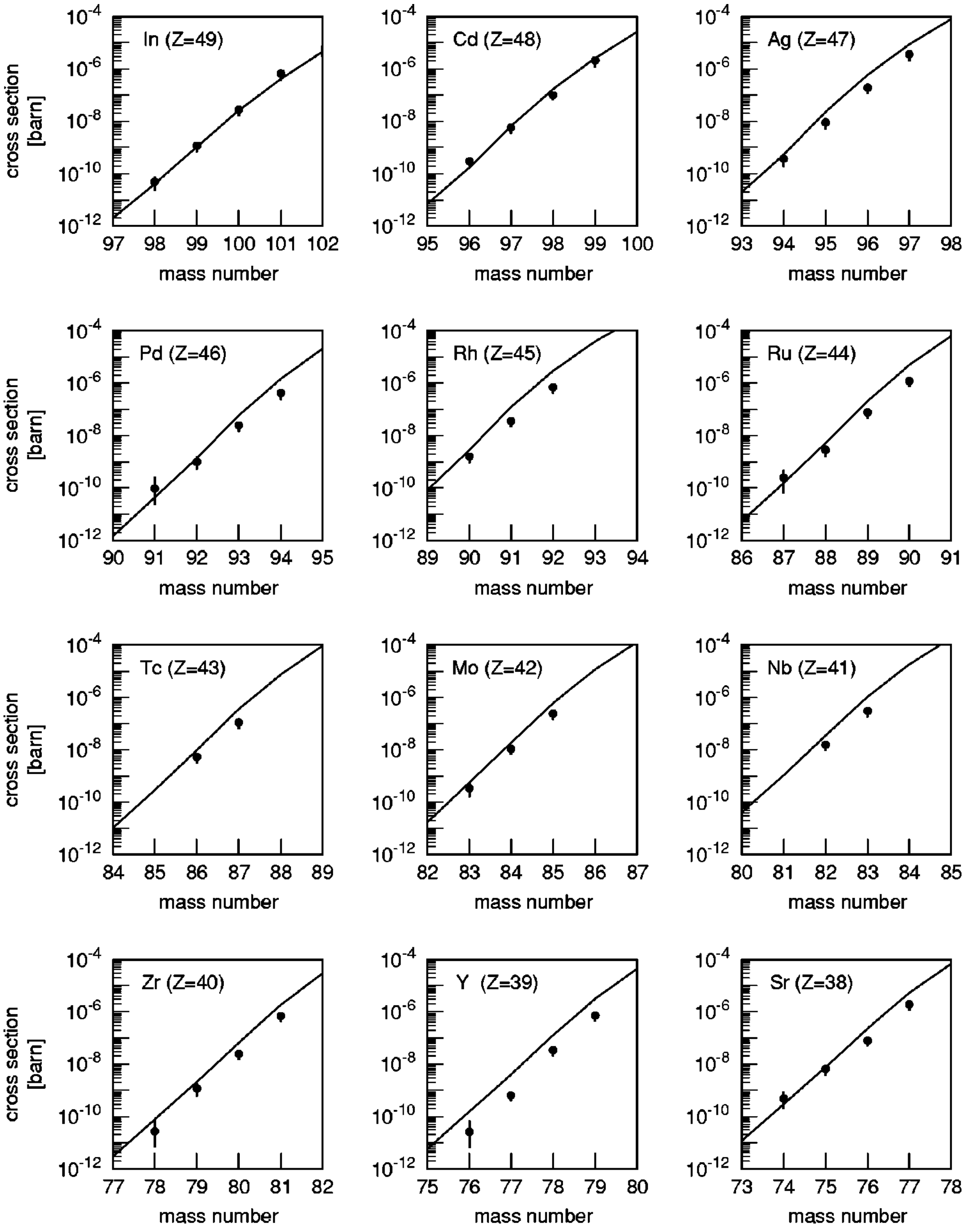

FIG. 5. Isotopic production cross sections for nucleon-removal channels from the reaction $1A$ GeV ^{112}Sn+^{9}Be. The solid lines indicate the prediction from the EPAX parametrization [18].

For the present target-projectile combination ^{112}Sn+^{9}Be, about 80 000 intranuclear cascades were run, followed by 5 independent evaporation sequences for each cascade. This allows us to calculate cross sections down to a level of about 10 μb. For the elements $_{50}$Sn and $_{49}$In, where there is sufficient overlap between the experimental and calculated isotope distributions, we show in Fig. 6 the results from our ISApace calculations by the open symbols. As in our previous studies, the experimental and simulated data match very well, indicating that the assumption underlying the ISApace approach of free nucleon-nucleon collisions followed by evaporation from an equilibrated compound nucleus is reasonable at least for the very peripheral collisions that contribute to the formation of the nuclides studied. Similar conclusions have recently been drawn from a much more comprehensive set of *exclusive* data, using also ISABEL to simulate the intranuclear cascade, by the EOS Collaboration [23].

We finally want to comment on the difference between ^{100}Sn formation cross sections from the present and the GANIL experiment [10], which amounts to a factor of $\geqslant 40$. Though the incident energies of $1015A$ and $63A$ MeV, respectively, are very different, there are indications that abrasionlike reaction mechanisms are at work in both regimes. This is based on the observation that the same EPAX curve that closely follows the measured production cross sections of neutron-deficient Ni fragments from $650A$ MeV ^{58}Ni fragmentation over nine orders of magnitude [9,24] matches well the observed formation cross section of the ten-neutron-removal product ^{48}Ni from $75A$ MeV ^{58}Ni fragmentation [25]. This cross section is only (0.05 ± 0.02) pb. On the other hand, a comparison of ^{86}Kr-induced fragmentation cross sections at $70A$ MeV [26] to the EPAX formula reveals a considerable excess, e.g., for the 12-neutron-removal product ^{74}Kr. The experimental cross section of (186 ± 46) μb contrasts with an EPAX prediction of only

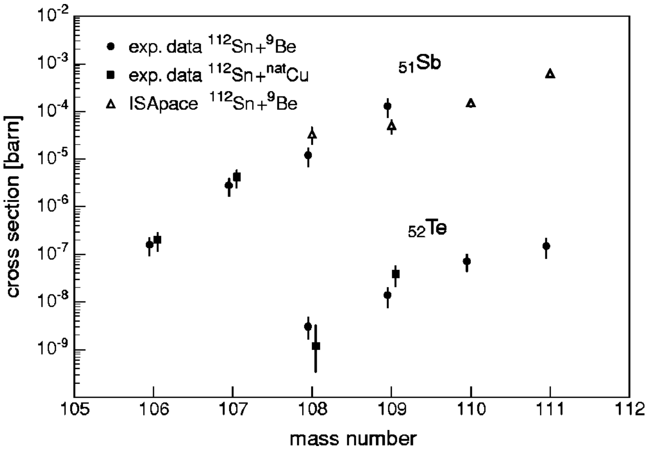

FIG. 6. Production cross sections for $(Z_{\mathrm{proj}}+1)$ and $(Z_{\mathrm{proj}}+2)$ charge-exchange products ($_{51}$Sb and $_{52}$Te isotopes) from the reaction of $1A$ GeV $^{112}_{50}$Sn+^{9}Be. Filled circles denote our experimental data. The open triangles are predictions for $_{51}$Sb calculated with the intranuclear-cascade plus evaporation package ISApace [19]. The filled squares are experimental data obtained with the Be target replaced by a Cu target (thickness 3976 mg/cm^{2}).

1.2 μb. It is not clear, however, if the influence of the incident energy plays a different role for neutron-rich and neutron-deficient projectiles. Thus it cannot be excluded that the difference in ^{100}Sn yield between the GANIL experiment and the present one is related to different reaction mechanisms at the two bombarding energies, though ^{112}Sn is almost as neutron-deficient as ^{58}Ni.

B. Cross sections of charge-pickup products

It is well known that even at relativistic beam energies, fragments are produced which have nuclear charges larger than that of the projectile. While most of the experiments performed can identify only the nuclear charge and not the mass numbers of the fragments (see, e.g., [27] and references therein), Sümmerer *et al.* [19] have measured isotopically resolved cross sections of $_{55}$Cs fragments from $^{129}_{54}$Xe $+^{27}$Al and compared them to ISApace calculations. The measured Cs isotope distribution could be well reproduced. The authors concluded that at incident energies of $\approx 800A$ MeV, (n,p) charge-exchange scattering and Δ excitation and decay contribute with about equal weights to the nuclear-charge pickup process. As a consequence, only masses equal to or lower than the projectile mass occur in the fragment distribution, and the cross sections are more than one order of magnitude smaller than those of neutron-removal products.

Similar observations can be made for the formation of $_{51}$Sb charge-pickup products (see Fig. 6). In addition to the $Z_{\mathrm{proj}}+1(_{51}\mathrm{Sb})$ isotopes, we could also detect $Z_{\mathrm{proj}}+2(_{52}\mathrm{Te})$ charge-pickup products. Note that the latter have cross sections almost four orders of magnitude smaller than the former.

Applying ISApace to the present target-projectile combination, we obtain the calculated cross sections for $^{108-111}$Sb shown by the open triangles in Fig. 6. The 80 000 intranuclear cascades that were run allow us to observe ^{108}Sb as the lightest isotope. Within the present statistics of the INC calculation, no $_{52}$Te events could be simulated. As in our previous study [19], the experimental and simulated data match very well, indicating as well that also the ratio of inelastic to elastic nucleon-nucleon collisions plus the time evolution of the intranuclear cascade has been described reasonably well.

V. SUMMARY

We have measured cross sections for projectilelike fragments close to the $N=Z$ line produced in the reaction ^{112}Sn+^{9}Be at an incident energy of $1A$ GeV. Cross sections of nucleon-removal products as low as a few pb could be measured. The results are in good agreement with the empirical parametrization of fragmentation cross sections, EPAX, except for isotopes of the projectile. The production of doubly magic ^{100}Sn by removing 12 neutrons from the ^{112}Sn projectile turned out to be less favorable compared to the removal of 20 neutrons and four protons from ^{124}Xe. This is in contrast to medium-energy reactions at GANIL where the former process was observed with a cross section that was larger by two orders of magnitude.

We could also measure isotopically resolved cross sections for one- and two-proton pickup which differ in magnitude by four orders. Intranuclear-cascade plus evaporation calculations reproduce the one-proton-pickup cross sections with good accuracy.

ACKNOWLEDGMENTS

The authors wish to thank K.-H. Behr, A. Brünle, and K. Burkard as well as the GSI workshop for technical assistance in the preparation phase. We also thank the accelerator crew of GSI for providing a high-quality ^{112}Sn beam.

---

[1] B.A. Brown and K. Rykaczewski, Phys. Rev. C **50**, R2270 (1994).
[2] J.C. Hardy, I.S. Towner, V.T. Koslowsky, E. Hagberg, and H. Schmeing, Nucl. Phys. **A509**, 429 (1990).
[3] H. Schatz, A. Aprahamian, V. Barnard, L. Bildsten, A. Cumming, M. Ouellette, T. Rauscher, F.-K. Thielemann, and M. Wiescher, Nucl. Phys. **A688**, 150c (2001).
[4] R. Schneider *et al.*, Z. Phys. A **348**, 241 (1994).
[5] R. Schneider *et al.*, Nucl. Phys. **A588**, 191c (1995).
[6] R. Schneider *et al.*, Phys. Scr. **T56**, 67 (1995).
[7] C. Longour *et al.*, Phys. Rev. Lett. **81**, 3337 (1998).
[8] E. Wefers, *et al.*, Phys. Rev. Lett. (submitted).
[9] B. Blank *et al.*, Phys. Rev. C **50**, 2398 (1994).
[10] M. Lewitowicz *et al.*, Phys. Lett. B **332**, 20 (1994).
[11] H. Geissel *et al.*, Nucl. Instrum. Methods Phys. Res. B **70**, 286 (1992).

[12] S. Kox, A. Gamp, C. Perrin, J. Arvieux, R. Bertholet, J.F. Bruandet, M. Buenerd, Y. El Masri, N. Longequeue, and F. Merchez, Phys. Lett. **159B**, 15 (1985).

[13] C. Ziegler, T. Brohm, H.-G. Clerc, H. Geissel, K.-H. Schmidt, K. Sümmerer, D.J. Vieira, and B. Voss, GSI Scientific Report 1990, No. GSI 91-1, 1991, p. 291.

[14] T. Stöhlker *et al.*, Nucl. Instrum. Methods Phys. Res. B **61**, 408 (1991).

[15] J.C. Santiard, W. Beusch, S. Buytaert, C.C. Enz, E. Heijne, p. Jarron, F. Krummenacher, K. Marent, and F. Piuz, Technical Report No. CERN-ECP/94-17, CERN, 1994.

[16] G.J. Feldman and R.D. Cousins, Phys. Rev. D **57**, 3873 (1998).

[17] N. Iwasa, H. Geissel, G. Münzenberg, C. Scheidenberger, T. Schwab, and H. Wollnik, Nucl. Instrum. Methods Phys. Res. B **126**, 284 (1997).

[18] K. Sümmerer and B. Blank, Phys. Rev. C **61**, 034607 (2000).

[19] K. Sümmerer, J. Reinhold, M. Fauerbach, J. Friese, H. Geissel, H.-J. Körner, G. Münzenberg, R. Schneider, and K. Zeitelhack, Phys. Rev. C **52**, 1106 (1995).

[20] Y. Yariv and Z. Fraenkel, Phys. Rev. C **20**, 2227 (1979).

[21] A. Gavron, Phys. Rev. C **21**, 230 (1980).

[22] K.-H. Schmidt *et al.*, Nucl. Phys. **A542**, 699 (1992).

[23] B.K. Srivastava *et al.*, Phys. Rev. C **60**, 064606 (1999).

[24] K. Sümmerer, W. Brüchle, D.J. Morrissey, M. Schädel, B. Szweryn, and W. Yang, Phys. Rev. C **42**, 2546 (1990).

[25] B. Blank *et al.*, Phys. Rev. Lett. **84**, 1116 (2000).

[26] R. Pfaff *et al.*, Phys. Rev. C **51**, 1348 (1995).

[27] C.J. Waddington, J.R. Cummings, B.S. Nilsen, and T.L. Garrard, Phys. Rev. C **61**, 024910 (2000).